PAPER AAS 93-552

Attitude Control of the Cassini Spacecraft During Propulsive Maneuvers

P. J. Enright

Jet Propulsion Laboratory

Pasadena, Calif.

AAS/AIAA Astrodynamics Specialist Conference

VICTORIA, B. C., CANADA AUGUST 16-19, 1993

AAS Publications Office, P.O. Box 28130, San Diego, CA 92198

AAS 93-552

Attitude Control of the Cassini Spacecraft During Propulsive Maneuvers

Paul J. bright*

The Saturn-bound Cassini spacecraft performs trajectory correction maneuvers using either the 0.6 N hydrazine thrusters of the reaction control system (RCS) or one of the two gimbaled 490 N bipropellant main engines. Preliminary designs arc presented for the algorithms which control the spacecraft attitude during these propulsive maneuvers, and also control maneuver termination. The RCS algorithm maintains the burn direction by off-pulsing the Av thrusters, and estimates the Av magnitude by monitoring thruster activity. The main engine algorithm is a thrust vector control (TVC) scheme which articulates the selected engine to stabilize the spacecraft altitude and maintain thrust vector pointing. For this case Av magnitude data is available from an integrating accelerometer and is used for closed-loop bum termination. 1 'or both algorithms, simulated performance is compared to the navigation requirements.

INTRODUCTION

The Cassini spacecraft (Fig. 1) is designed for a four-year orbital tour of the Saturn system, with delivery of the Huygens Probe (ESA) into the atmosphere of Sat urn's largest moon, Titan. Cassini is scheduled for an October 1997 launch on a Titan 1 V / Centaur upper stage combination. The mission design includes gravity-assist flybys of Venus, Earth, and Jupiter, and eventual rendezvous with Saturn in June 2004. The interplanetary cruise trajectory requires a large maneuver between the Venus flybys, and as many as twenty smaller trajectory correction maneuvers (TCMs) for navigation. The orbital phase begins with the long Saturn-m-hit insertion burn just after periapse, followed by a periapse-raising maneuver at apoapse, which establishes the initial tour orbit. The probe is released on a T'i tan i mpact trajectory, and after performing a small deflection maneuver, the orbiter records the probe data as it enters Titan's atmosphere. The orbital tour include-s many small TCMs, targeting the orbiter for flybys of Titan and the icy satellites Rhea, Dione, Iapetus, and Enceladus.[1]

The bulk of the maneuver Av required for the mission is delivered by the (selected) main engine, a 490 N bipropellant thruster, which burns MMH and N_2O_4. (There arc two identical main engines for redundancy.) At launch, the total bipropellant load is 3000 kg, which is a bit over 60% of the spacecraft's launch mass. The separate Reaction Control System (RCS) consists of sixteen 0.6 N monopropellant thrusters (eight redundant pairs) fed by a single tank which contains 132 kg of hydrazine at launch. The RCS is used for

* Member Technical Staff, Jet Propulsion Laboratory, California Institute of Technology, Pa.sactcaa,CA91109

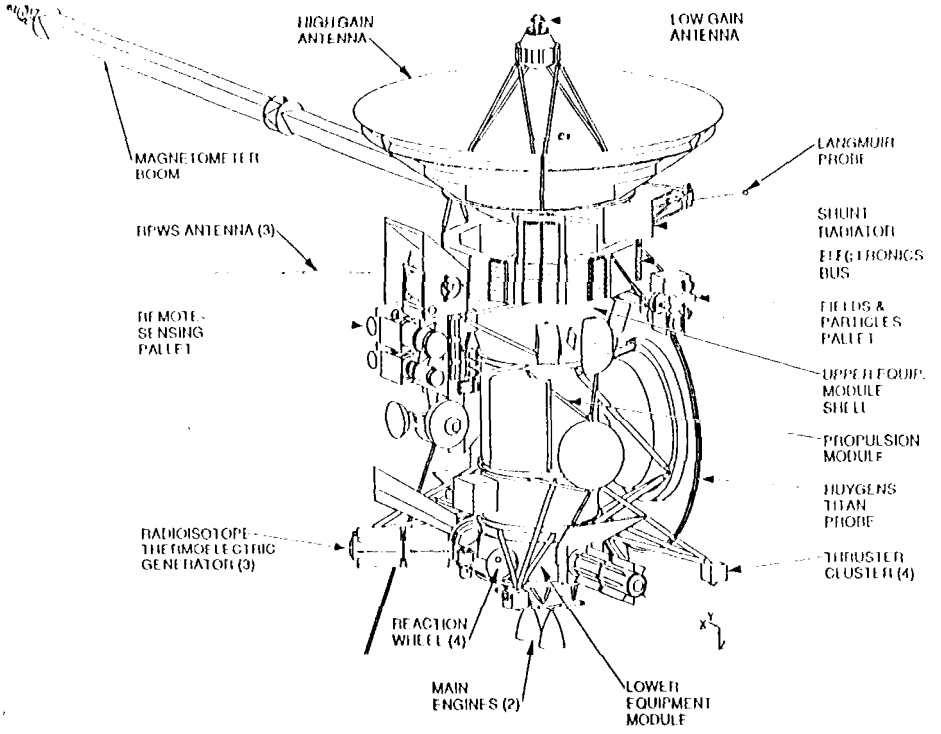

Fig. 1 The Cassini Spacecraft

cruise attitude control and for momentum management during the orbital phase when the reaction wheels arc in USC. The Z-facing RCS thrusters arc also used for small Av maneuvers.

'l'his paper describes preliminary designs for the RCS Av algorithm and the main engine Av algorithm. These algorithms control the spacecraft attitude during the maneuvers and also control maneuver termination. First, the overall architecture of the attitude control system is presented, followed by descriptions of vehicle dynamics and sensor models. Next, the design of each algorithm is presented separately, including actuator models, control law synthesis, and margin analysis, with special attention paid to interactions with structural flexibility and propellant dynamics. Common-platform simulation results arc presented and evaluated in the context of the maneuver crmr specifications required by the navigation group.

ATTITUDE CONTROL ARC I IITECTURE

The attitude control software has been organized as a collection of "objects," with carefully managed data flow between them.[2] Figure 2 depicts the subset of these software modules which support Av maneuvers, and provides a useful format for (discussing the overall system architecture. The Attitude Estimator maintains a 3-axis attitude estimate using data from the Inertial Reference Unit (1 RU) Manager, which is the interface routine to the gyro package. This estimate is updated using celestial measurements provided by Star ID, which is the interface to the star tracker. A single integrating accelerometer provides an estimate of the Av along the spacecraft 7.-axis. The Attitude Estimator sends 'the current spacecraft attitude quaternion (with respect to the inertial J2000 frame), q^e, and angular

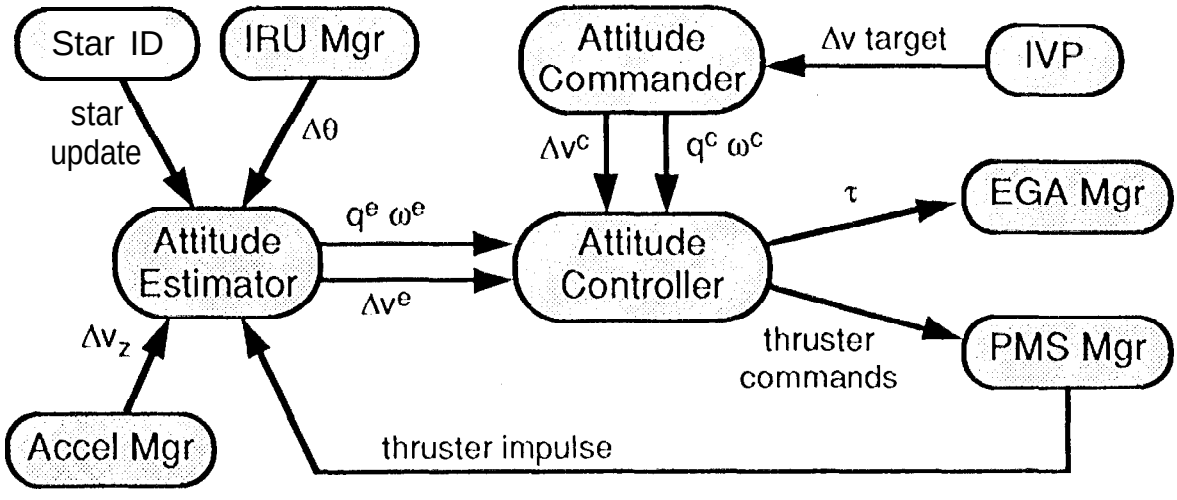

Fig. 2 Control Architecture

velocity, ω^e, to the Attitude Controller, along with an estimate of the accumulated Av. The Attitude Controller compares this data to the commands coming from the Attitude Commander, and takes the appropriate action. Thruster commands arc sent to the PMS Manager, which interfaces to the electronics which drive the valves of the Propulsion Module Subsystem. During main engine burns the Attitude Controller also sends engine articulation commands to the EGA Manager, which interfaces to the electronics which drive the Engine Gimbal Actuators to provide the requested thrust vector, τ.

A functional breakdown of the Attitude Controller object is depicted in Fig. 3. The error generation function derives the single-axis attitude and rate error 3-vectors, p and r, as follows:

$$p = 2\xi \tag{1}$$

$$r = \omega^c - \omega^e \tag{2}$$

where ξ is the modified error rotation vector computed from the error quaternion:

$$\xi_i = [q^{e,c}]_i \, \mathrm{sgn}([q^{e,c}]_4) \tag{3}$$

with $q^{e,c} = q^e(q^c)^*$ (The asterisk denotes conjugation, juxtaposition denotes quaternion multiplication, and $[\ ]_i$ denotes the i^{th} element.) The attitude error p is accurate only for small angles, but never singular. The single-axis errors arc passed on to the active controller, either the RCS Av algorithm, or the main engine Av algorithm, which arc discussed in detail below. (Note that Fig. 3 shows only these maneuver modes, excluding both the RCS attitude control algorithm which controls the spacecraft attitude during the interplanetary cruise phase, and also the reaction wheel attitude control algorithm, which operates during the orbital phase.)

The Attitude Controller also compares the estimated maneuver Av to the commanded Av, and terminates the maneuver appropriately. The estimation of the maneuver Av and

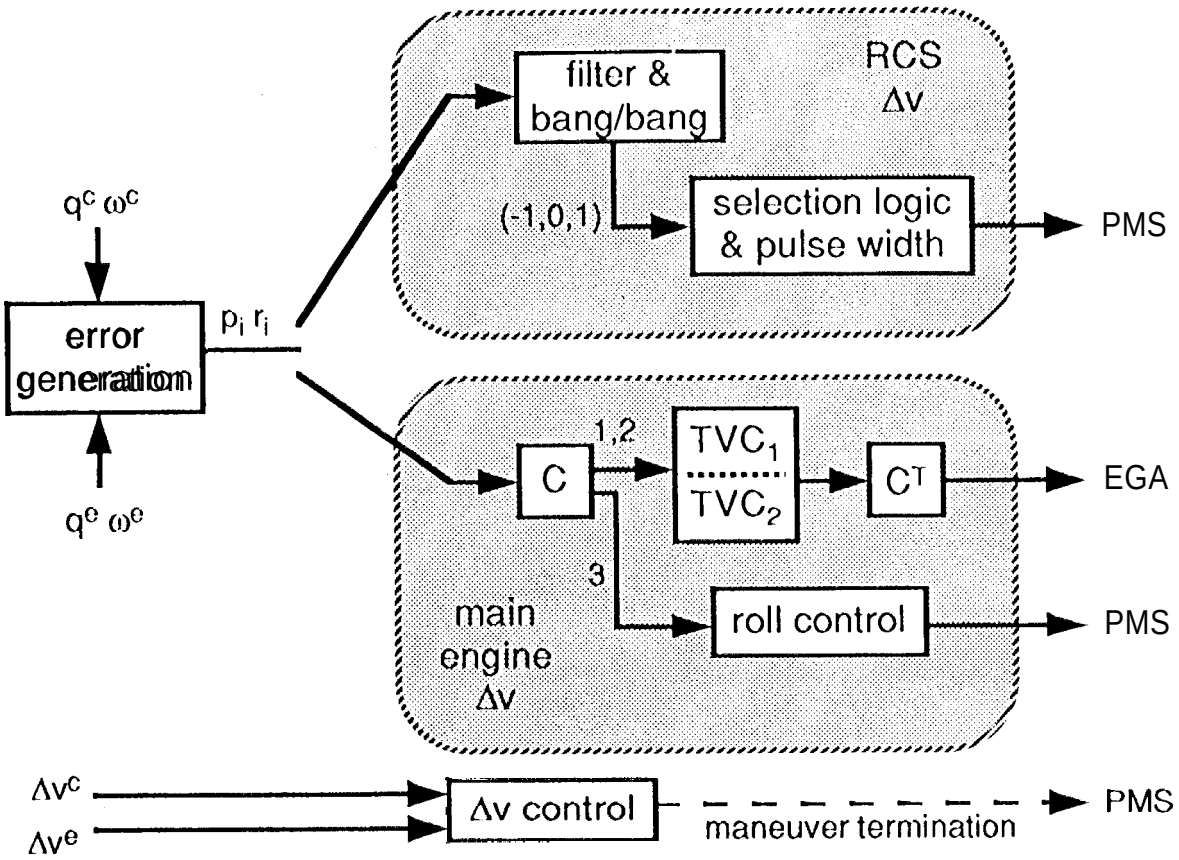

Fig. 3 Attitude Controller

also the termination logic are different for the two algorithms, and the designs are discussed separately below.

VEHICLE DYNAMICS

The spacecraft structure is designed around the propulsion module, which houses the two bipropellant tanks (cylindrical with hemispheric heads) in a stacked configuration. Each tank includes a propellant management device (PMD), which exploits surface-tcnsicm forces to control the propellant center-of-mass under quiescent conditions. The upper and lower equipment modules attach to the propulsion module (Fig. 1), forming the central structure of the spacecraft, which can be considered rigid in this analysis. Most of the longcron-supported equipment is also very stiff, with resonant frequencies typically 10 Hz and above. Exceptions arc the 10-meter magnetometer boom, whose first bending mode is constrained to be above 0.7 Hz, and the three light RPWS antennas, with first bending modes near 0.13 Hz.

For the current study, it is adequate to model the spacecraft structure as a rigid "basebody" with a spring-restrained appendage for the mag boom, the 1 kg RPWS antennas not being large enough for concern. The mag boom spring constant is chosen to

match available finite-clcmcnt data, and the damping is amplitude dependent, ranging from 0.25% at small amplitudes to 1% at large amplitudes. (This is based on experimental data from the Galileo mag boom, which is similar.) For RCS Av's, the bipropellant is modeled as spring-restrained masses, each attached to a point along the centerline of the corresponding tank, which mimics the "centering" effect of the PMD in the low-g environment. Spring constants and attachment points arc derived from quasi-static data generated using a program which solves for minimal surfaces in the presence of surface tension and gravity.[3] This "low-g" model has frequencies near 0.01 Hz, and damping estimates anywhere from 0.2% to 5%. The relatively high acceleration associated with main engine Av's makes surface tension forces irrelevent, and the bipropellant is modeled as pendulums with mass, length, and attachment point computed using potential flow solutions. (Analytical results[4] arc supplemented by CFD results where possible.) Under the main engine acceleration, the bipropellant pendulums "slosh" near 0.1 Hz. For simulation, the system equations of motion were generated by a symbolic manipulation code.[5] In future studies, a higbcr-fidelity model will be used, which incorporates the mag boom and RPWS flexible modes (as well as any other significant flex modes) into a central flexible basebody.[6]

ATTITUDE ESTIMATION

The strap-down integrating gyro package is mounted to the upper equipment module (Fig. 1). Every computational cycle (125 ms) the gyro manager reads the time-tagged angular increments accumulated since the previous reading. (One pulse corresponds to 8 μrad of rotation.) The attitude estimator propagates the spacecraft quaternion using a second-order expansion of the quaternion kinematic equation, and derives rate using the first-order difference. The dynamics of the gyro rebalance loop arc modeled as a damped second-order system with a 5 Hz bandwidth, and an integral pole at 0.51 Iz. White noise inputs in acceleration and rate integrate. to rate and position random walks. Although the simulation model includes the pulse-generation logic, the linearized "design model" ignores the quantization altogether, 8 μrad being negligibly small in the maneuver environment.

During RCS Av's, the spacecraft is in "cclcstial-inertia]" mode, with the gyro-propagated attitude estimate being updated once a second by prefiltered celestial measurements from StarID. Celestial updates may not be available during main engine Av's duc to the relatively high spacecraft rates. As a result, for long main engine burns, the integrated gyro errors dominate the Av pointing error budget.

TURNS-TO-BURN

For RCS Av's, the thrust acceleration is along the spacecraft -Z-axis. Prior to the burn, the spacecraft must be reoriented to point the -Z-axis along the Av vector requested by the navigation team. This can be done using either the RCS attitude controller, or the reaction wheel attitude controller. For RCS turns the usc of unbalanced thrusters results in a "turn-residual" Av, whose magnitude and orientation depends on the turn rate and geometry. 'l'his Av is factored into the maneuver design, and also the expected prediction error is included in the maneuver accuracy budget. (Significant uncertainties arise duc to interaction with the sloshing bipropellant.) For main engine burns, the situation is similar, with the exception that the maneuver attitude must point the "pre-aim" vector at the Av target. The pre-aim vector is from the selected main engine to the center-of-mass, and defines the initial engine articulation.

RCS AV

RCS burns arc initiated by firing the four Z-facing RCS thrusters. The X and Y attitude is maintained by "off-pulsing" these thrusters, while the Z-axis is controlled by pulsing the X-facing thrusters which arc arranged in couples. For the X and Y axes, the primary disturbances arise from the center-of-mass offset from the Z-axis, and thruster-to-thruster performance variations. For rotation about the Z-axis, the only significant disturbance is due to the misalignments of the Z-facing thrusters.

The single axis position and rate errors, pi and r_i from eqs. (1) and (2), arc combined with a lead time constant k_r:

$$c_i = p_i + k_r r_i \tag{4}$$

and then low-pass filtered. (The Z-axis error is not filtered.) The filtered errors drive the bang-bang control logic to produce torque polarity requests (-1,0, or 1 for each axis):

$$n_i = \mathrm{sgn}(c_i) \text{ if } |c_i| > d_i \text{ , else } n_i = 0 \tag{5}$$

where d_i is the deadzone half-width. The torque polarity requests arc then processed by the thruster selection logic defined by the tables in Fig. 4. The thruster nomenclature is as shown in the figure to the right, which shows the spacecraft viewed from the +Z direction. (The Z thrusters arc spraying hydrazine toward the viewer.) Note that an X or Y deadzone violation alone causes a pair of Z thrusters to off-pulse, while a combination results in off-pulsing of a single thruster. Z deadzone violations result in pulsing X thruster couples.

The low-pass filtering of the X and Y error signals was introduced to prevent high-frequency chatter about a switch line duc to the presence of the constant disturbances from the center-of-mass offset. The filtering results in longer off-pulses, improving thruster efficiency and reducing the number of thruster valve actuations which is considered to be a "consumable." The current .sccond-order filter design has a pair of underdamped poles at 1 rad/s. Although the controller runs every 125 mscc, the hardware supports scheduling of

X/Y off-pulse (125 ms)

	Y = -1	Y = 0	Y = +1
X = -1	Z4	Z3&Z4	Z3
X = 0	Z1&Z4	none	Z2&Z3
X = +1	Z1	Z1&Z2	Z2

Z on-pulse (25 ms)

Z = -1	Z = 0	Z = +1
X2&X4	none	X1&X3

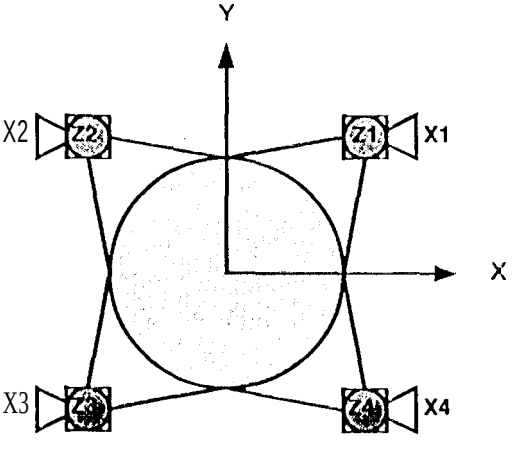

Fig. 4 Thruster Selection Logic

thruster valve commands to a much finer resolution. The PMS manager has been designed to accommodate not only "on" and "off' commands, but also commands of the type "on for t msec." For X and Y axis control (Z thrusters), the "off" command is used, since the 125 msec resolution is more than sufficient, and typical off-pulses last several seconds. However, Z-axis control (X thrusters) uses the "on fort m.see" format with t set to provide the minimum impulse bit which the thruster can support. 'l'his minimizes wasteful two-sided limit-cycle activity in the low-disturbance environment,

It has been assumed that the computational delay between reading of the gyros and the subsequent issuance of thruster valve commands is the entire 125 mscc cycle, although this is expected to improve considerably as the software and processor performance become better defined. The only other significant time delays arc those associated with thruster transients, and arc expected to be on the order of 1 00 msec. The current value chosen for the lead constant k_r of cq. (4) is 3 seconds, so rigid-body stability is not an issue. There arc a few non-rigid dynamics concerns, namely the low-g bipropellant slosh modes near 0.01 Hz, and the lightly-damped magnetometer boom bending mode at 0.71 Iz. For the Cassini geometry, the low-g slosh modes arc "stably-interacting" in the RCS Av mode, meaning that they arc stabilized by a controller of the proportional-plus-derivative type with no significant actuator dynamics or time delays. (In general, for control with unbalanced thrusters, internal flexibilities can be unstably-interacting.[7]) Because timing delays contribute a negligible phase lag at low frequencies, the modes arc not a concern from a stability point of view, although they do cause significant disturbances during and after turns, and somewhat corrupt the predictability of the turn-residual Av. Although appendage-type modes like the magnetometer boom bending arc stably-interacting, they can be destabilized by actuator dynamics and timing delays. The phase lag duc to the 125 mscc computational delay combined with a 100 msec thruster lag is already 57° at the mag boom frequency of 0.7 Hz. The low-pass filtering of the X and Y errors alleviates this concern somewhat, effectively gain stabilizing the bending mode. The situation can be quantified by replacing the bang-bang controller with its describing function equivalent gain. Letting Ml be the X-axis moment from the Z3/Z4 combination, the equivalent gain is:[8]

$$k_b = \frac{2M_1}{\pi d_1} \tag{6}$$

With the rigid body plant and the lead compensation only, the open-loop transfer function becomes:

$$I,(s) = \frac{(k_r s+1)}{s^2} k_b \tag{7}$$

and for high frequencies, say $\omega > 1$ rad/s, the gain is approximately $\frac{k_r k_b}{I\omega}$. For two 0.6 N thrusters at a 1.57 m moment arm, Ml = 1.88 Nm. The deadzone of 2 mrad results in k_b = -598 Nm/rad. Using the, end-of-mission X-axis moment-of-inertia of 5378 kgm^2, the gain at 0.71 Iz becomes 0.076, or -22 db. NASTRAN data (with the assumed 0.25% damping) indicates that the bending mode has a peak of almost 30 db. The low-pass filter contributes -13 db attenuation at the mag boom frequency, but this leaves only 5 db of margin. The Z-axis situation, with no filtering, is still phase-stable (the nominal delays arc not large enough to kill the 90° of lead from the rate gain), but possibly sensitive to thruster characteristics. The whole picture needs to be re-assessed as timing estimates and thruster data become available. Alternate schemes to extend off-pulse durations (without filtering) arc currently being investigated. A particularly attractive approach would be to manipulate

pulse sizes using a disturbance estimate, which may also be useful during RCS attitude control.

The accelerometer bias is probably not sufficiently stable to provide an accurate Av estimate during RCS burns. (The accelerations are as low as 50 pg.) Instead, Z.-thruster activity is monitored and the thrust impulse is estimated as a function of total on-time and number of on/off switches. The low-pass filtering keeps the off-pulses large enough so that tail-off transients from an "off" command arc not interrupted by a subsequent "on" command, and this keeps this scheme simple and accurate. As thruster test data becomes available, this model may be enhanced to capture the slow increase of the steady-state thrust level as the thrusters warm up during the tour.sc of the maneuver.

The RCS controller was integrated into a common simulation platform built around the multi-body spacecraft dynamics model. The thruster model uscs exponential force profiles based on the rise-time and tail-off specifications. Also included were preliminary versions of the PMS Manager and the Attitude Estimator, along with the gyro model. Fig. 5 shows tbc attitude errors P_i, for a lo-minute burn, which imparts 0.5 m/s to the spacecraft. Note the higher frequency activity on the Y-axis, which is duc to the large X center-of-mass offset. Fig. 6 shows the Z-thruster activity over the first minute.

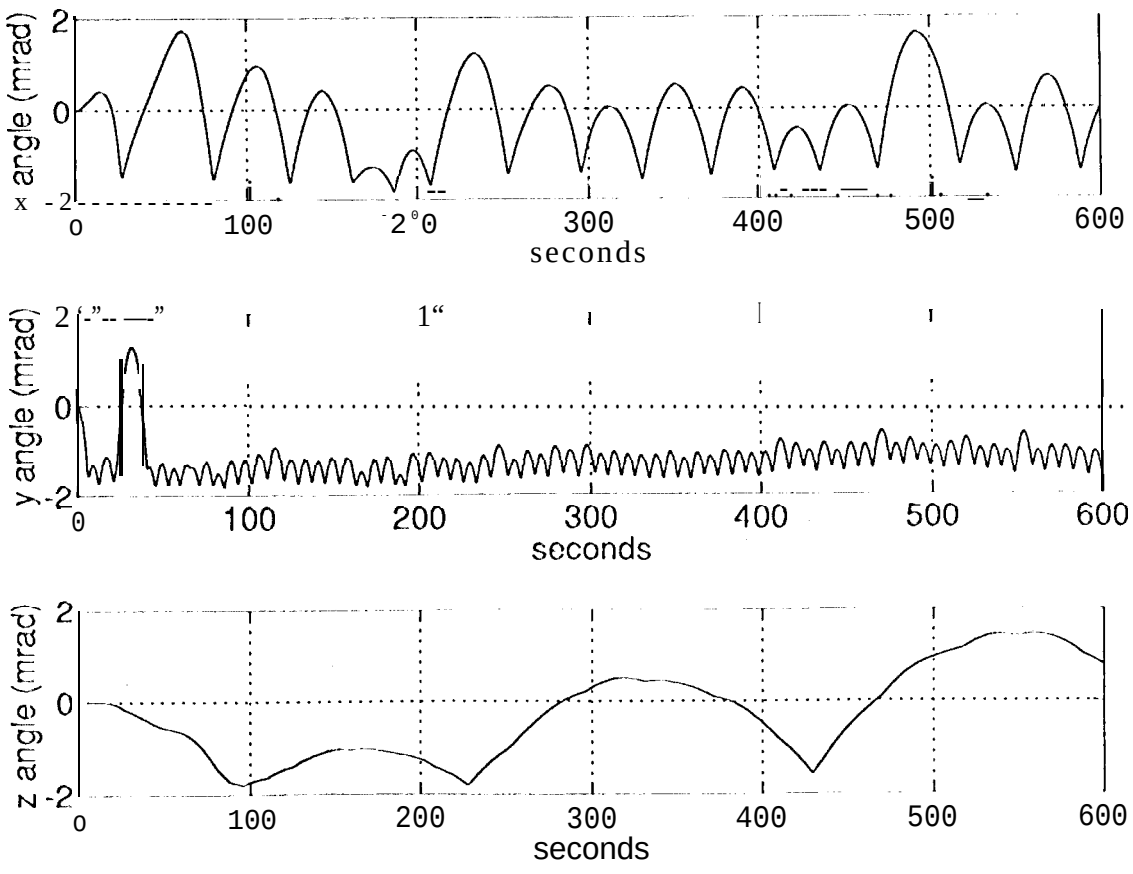

Fig. 5 RCS Av Simulation **(Attitude)**

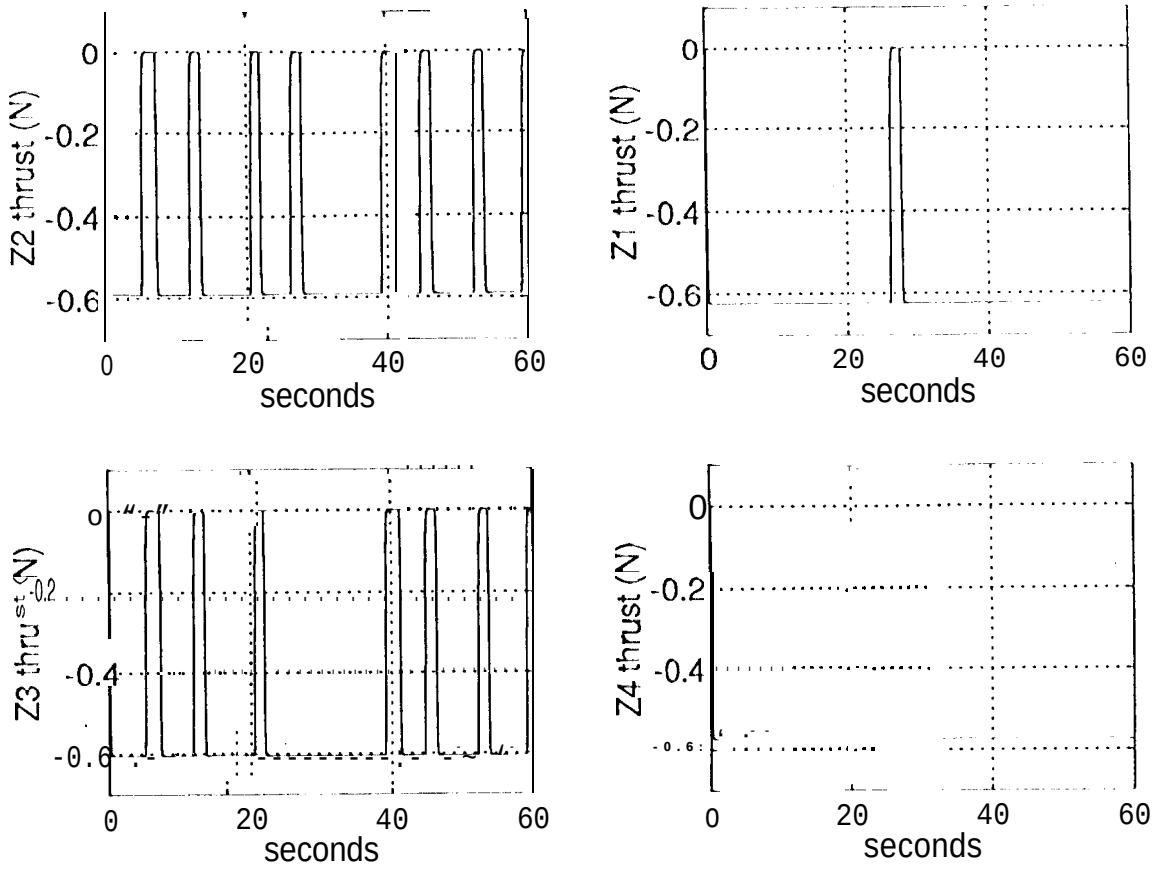

Fig. 6 RCS Av **Simulation (Thruster Activity)**

Tables 1 and 2 summarize the maneuver error budgets, which are 3σ errors for an assumed normal distribution. Magnitude errors arc along the target Av, while pointing errors arc orthogonal. The errors arc further broken down into contributions which arc fixed in size, and those which arc proportional to the Av magnitude. Note that the fixed errors arc dominated by the limited predictability of the turn-residual Av, although this is clearly not an issue when the turn-to-burn is performed on the reaction wheels. The proportional errors arc dominated by uncertainties in thruster characteristics, namely performance variations and misalignments.

error source	fixed error (mm/s)	proportional error (%)
probabilistic turn-residual ΔV [type-2 @0.25 deg/s]	3.0 (0.0)+	----
impulse prediction uncertainty		
uncorrelated	----	3.56
correlated	----	2.5
spacecraft mass uncertainty	----	2.2
maneuver termination resolution	0.13	----
RCS residual rate	0.94	----
TOTAL (RSS)	3.1 (1.0)+	4.9
REQUIREMENT	10,5	6.0

+ turn performed on wheels

Table 1 RCS ΔV Magnitude Errors (3σ)

error source	fixed error (mm/s)	proportional error (mrad)
probabilistic turn-residual ΔV [type-2 @0.25 deg/s]	3.0 (0.0)+	----
initial attitude determination	----	4.0 (5.7)*
gyro scale factor / misalignments (1 80° turn)	----	1.6 (19.9)*
thruster misalignments:		
uncorrelated	----	7.57
correlated	----	5.0
basebody attitude control:		
X-Y control	----	5.0
roll control	----	0.76
TOTAL (RSS)	3.0 (0.0)+	11.2 (23.2)'
REQUIREMENT	10.5	25.5 (36.0)'

+ turn performed on wheels
* uncalibrated

Table 2 RCS ΔV Pointing Errors (3σ)

MAIN ENGINE AV

Each main engine is mounted to the "bottom" (+Z) of the spacecraft in a gimbal system, allowing two axes of articulation for thrust vector control (TVC) during burns. The third axis (roll about the thrust vector) is controlled using the X-facing RCS thrusters. For a three-axis stabilized spacecraft, the primary advantage of the gimbaled engine design is that it eliminates the need for intermediate-sized thrusters dedicated to attitude control during the burn. The block-redundant Cassini design also provides single-fault tolerance for the engine and its gimbal actuators, which must perform as many as 100 burns over the 11-year mission.

The main engine Av algorithm first transforms the single-axis position and rate errors, p_i and r_i, into a coordinate system which has it's -3-axis aligned with the pre-aim vector, τ_0. At launch, the pre-aim vector is the ground estimate of the unit vector from the main engine to the spacecraft center-of-mass, and the main engine is articulated along this vector just prior to ignition. Engine gimbal telemetry during the burn can be used to update the pre-aim vector to improve the performance of subsequent maneuvers. Let C be the rotation matrix such that the transformed errors become:

$$p^{TVC} = C(\tau_0)p \qquad r^{TVC} = C(\tau_0)r \tag{8}$$

The 1 and 2 components of the transformed errors drive two single-axis TVC controllers, which output angular acceleration commands, $a = [a_1\ a_2]^T$. These are translated into engine rotation commands β_1 and β_2 as follows:

$$\beta = \frac{I_R a}{fd} \tag{9}$$

where I_R is the upper left 2x2 partition of the inertia matrix transformed into the TVC coordinates, f is the main engine force, and d is the distance from the main engine to the center-of-mass. The small rotations β are assembled into a unit vector and transformed back into spacecraft coordinates:

$$\tau_c = C^T [-\beta_2\ \ \beta_1\ -1]^T \tag{10}$$

"This commanded thrust vector is passed to the EGA Manager, where it is transformed into a coordinate system associated with the selected main engine. The engine coordinate system has its 1- and 2-axes aligned with engine gimbal axes and its 3-axis along the thrust vector when the actuators (EGAs) are at their null extension. After calculating the gimbal angles necessary to align the engine to the commanded thrust vector, the manager converts these angles to appropriate actuator extension commands. This conversion is not trivial, since the actuator/gimbal geometry makes a linear approximation less than acceptable.~

The 3-component of the transformed position and rate errors are passed to a bang-bang controller identical to the Z-axis controller used for the RCS Av. A wide deadzone of ± 10 is used to prevent unnecessary thruster activity during burn transients. Note that the X-thruster couples provide torque about the Z-axis rather than the thrust vector which may be several degrees from the Z-axis, although the resulting perturbation to the 1- and 2- axes is negligible.

The two single-axis TVC controllers are identical, and control about the 1-axis, which is close to the spacecraft X-axis, is now presented in detail. Fig. 7 shows the linearized

model which was used for TVC design. (Fig. 8 is a blow-up of the block labeled TVC_1.) As depicted the output of the TVC block is a gimbal angle command, which is delayed, held, and passed through a first-order lag to result in the engine gimbal angle. obviously this is a gross simplification of the data flow between TVC and the EGA manager outlined above. "l'he first-order lag is intended to bound the phase lag from the EGA servo, which was determined by a detailed simulation of the actuator and the digital servo electronics. The gimbal angle of Fig. 7 is relative to the initial thrust vector orientation, and drives the spacecraft dynamics model after being augmented by the "pre-aim" error ε, which is the angle between the initial engine thrust vector and the vector from the engine gimbal through the system center of mass. (Due to mass property uncertainties and various misalignments, this can be as large as 1° for the first burn.) The spacecraft dynamics model is a cascade of the transfer functions, evaluated at current mass property estimates for a 50% bipropellant fill. Included arc the mag boom bending mode, the coupled bipropellant slosh modes, and the rigid body mode which has been combined with the tail-wags dog zero associated with the main engine inertia.g The output of the double-integrator is the basebody angle, which feeds the 3rd-order gyro model. At this point the sensed angle is sampled and sent to the controller, along with the back-differenced rate estimate. This is a simplification of the process which occurs in the attitude estimator, the attitude commander, and the error generation block of Fig. 3, which is made possible by the single-axis reduction and the restriction to small errors. Note that it has been assumed here that the commanded position and rate arc both zero.

As is evident from Fig. 7, the pre-aim error ε comes in as a constant disturbance, and the s ystem response to this deserves some attent ion. The physics of the problem dictates that the steady-state situation has the thrust vector pointing through the system center of mass, i.e. $\gamma_{ss} = -\varepsilon$. The necessary basebody pointing error to drive this offset would be $\theta_{ss} = \varepsilon/k$, where k is the position-to-gimbal gain, and the resulting thrust vector would be rotated by $(1 + 1/k)\varepsilon$ with respect to its initial orientation. This error is unacceptable, and is remedied by positive feedback of the commanded gimbal angle with a gain of $1 + k$, as shown in Fig. 8, which makes the steady-state, gain from θ_c to γ equal to -1. This design was adapted from the analog Mariner 9 design,[10] where it was termed "path-guidance," it being viewed as a rather degenerate form of the more general "guidance loop" associated with missile autopilots. The guidance loop adds a zero and a right half-plane pole, providing 180° of phase shift at low frequencies. This is necessitated by the fact that the transfer function from y to the "inertial" thrust vector, $\theta + y$, is non-minimum-phase.

"1'here is a clear desire to maintain the controller bandwidth as large as possible, not only to minimize the maneuver errors, but also to keep spacecraft rates to an acceptable level during the transient that follows ignition. (This is a problem particularly for short burns, where even a moderate rate following engine cut-off may be difficult for the low-authority RCS thrusters to cope with.) Sensors and actuators arc flat out to a few Hz, and the Nyquist frequency is at 4 Hz, suggesting that the system is equipped to operate up to 0.4 Hz or so without difficulty. "l'his is complicated, however, by the presence of the lightly-damped magnetometer boom bending mode near 0.7 Hz. As mentioned above, this mode is benign in the sense that it interacts stably with an infinite-bandwidth PD controller. But for the system at hand, the phase situation starts to degrade rapidly around 1 Hz, with significant losses resulting from sensor/actuator dynamics, the need to derive rate by back-differencing position, and the proximity of the Nyquist. 'l'his is exacerbated by the computational delay of 125 msec (an entire sampling period), which at 1 Hz already contributes 45° of phase lag. This situation prompted a decision to gain-stabilize the mag boom mode.

The following design margins were adopted: 30° phase lead over ±6 db, and 12 db gain margin at the mag boom resonance peak, which is 18 db high for 1 % damping. The gain curve should cross 0 db at a steep -10 db/oct, flatten out at the lower gain margin to maintain the phase lead, and then roll off sharply, in this case at -18 db/oct. (This is the fastest possible cut-off which maintains the stability margins.[11-12]) Backing off from the mag boom requirement, this puts the crossover at 0.1 Hz, an ideal location in terms of the bipropellant slosh, since it provides excellent margins for frequency uncertainty (better than a factor of two in either direction.) A 7th-order compensator was synthesized to follow the Bode cut-off, and then digitized for the 8 Hz sampling. (The symbol $Z\{\}$ in Fig. 7 denotes a discrete equivalent via bilinear transform.) The continuous version is as follows:

$$\frac{c(s)}{D(s)} = 18.7\ \frac{(s^2+.19s+.026)(s^2+1.2s+1)(s+.7)(s+1.6)}{(s+.5)(s^2+.8s+.19)(s+1.2)(s+1.89)(s^2+1.88s+3.53)(s+k_r)} \qquad (11)$$

Note that the $(s+k_r)$ term in the denominator removes the effects of the separate rate gain from the loop transfer function, leaving k_r free to be chosen as a prc-filter parameter. ('l'his can be used to optimally mix the position and rate estimates, which could have different noise characteristics if StarID is providing updates.) As indicated in Fig. 8, the DC gain of the controller is 1 (deg/deg). The guidance loop time constant was set to 10 seconds; faster values interfere too much with the phase near cross-over. Figures 9 and 10 show the complete open-loop frequency response. The closed-loop bandwidth is 0.23 Hz.

Every computational cycle during the burn the attitude estimator polls the accelerometer for the Z-axis Av accumulated since the previous read. (The resolution is 0.2 mm/s.) These arc summed, and the total is divided by the cosine of the angle between the Z-axis and the pre-aim vector. This compensated estimate is passed to the Attitude Controller, where it is compared to the commanded Av magnitude. The controller calculates the "burn-time-to-go" based on the remaining Av and nominal thrust level and spacecraft mass. When this is less than a computational cycle, the controller schedules main engine valve closure accordingly. Note that sometime prior to the main engine burn the Accelerometer Manager is commanded to autonomously calibrate the bias error by reading data during a quiescent period, and making the. necessary adjustment.

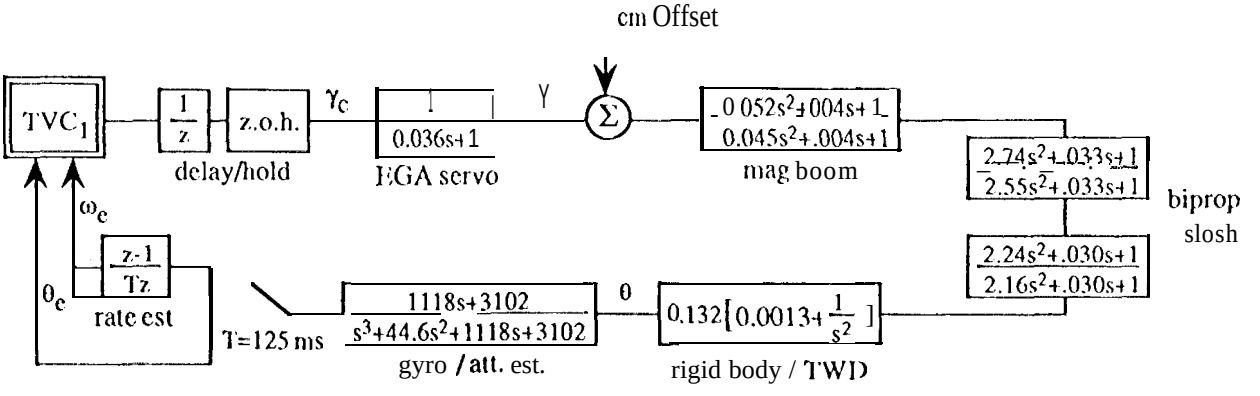

Fig. 7 TVC 1 Block Diagram

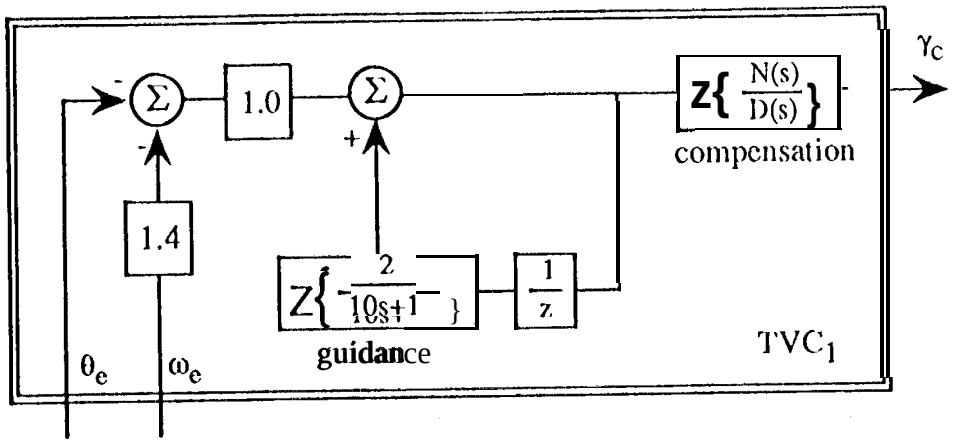

Fig. 8 TVC_1 Controller

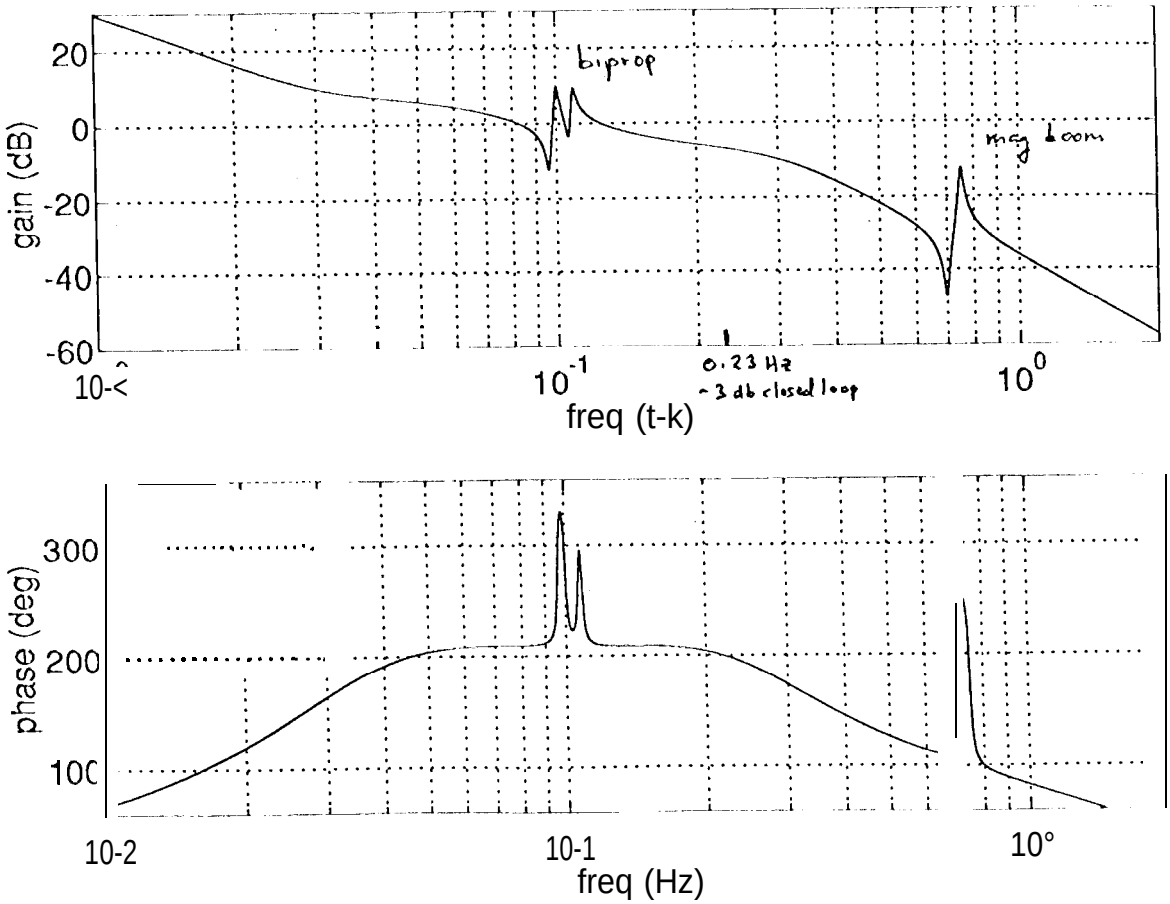

Fig. 9 TVC Frequency Response

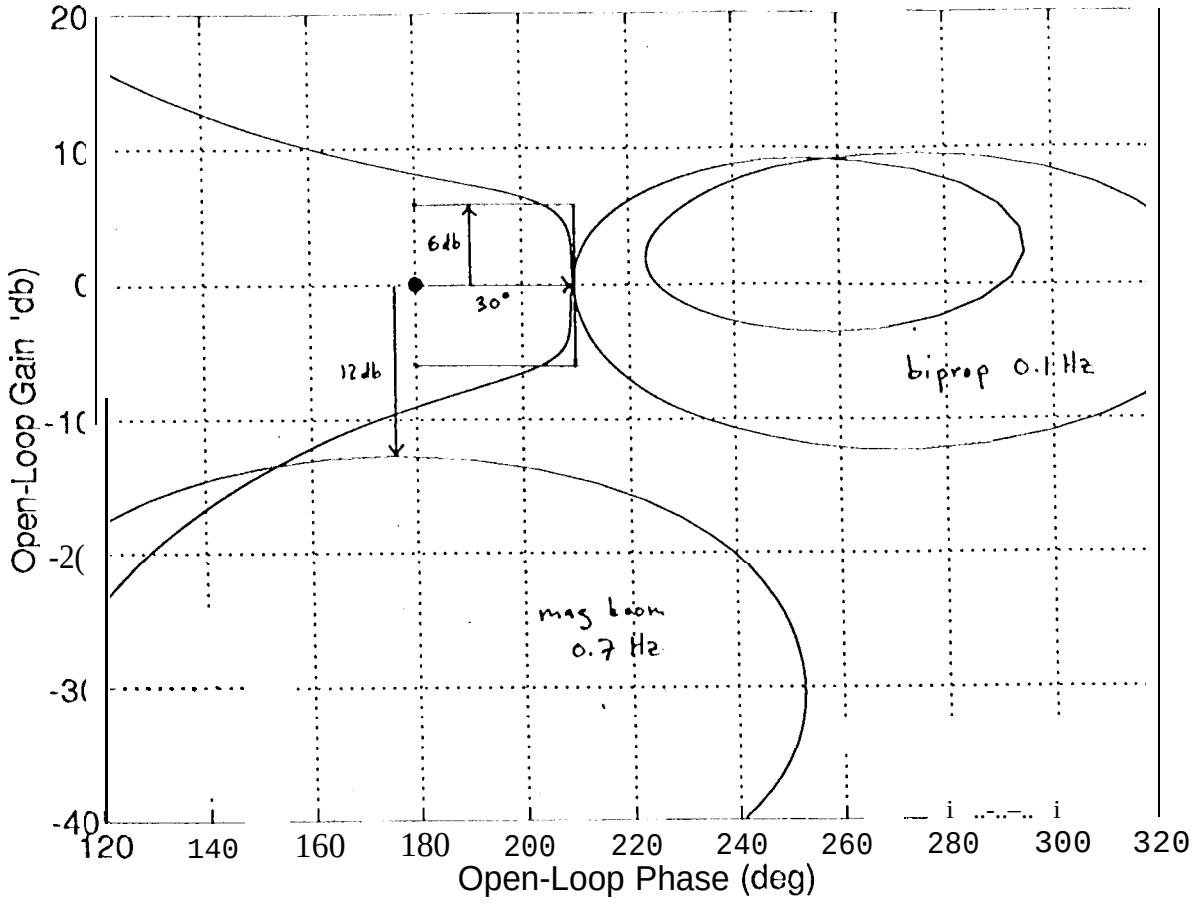

Fig. 10 TVC Nichols Chart

The controller was integrated into the simulation platform with the hardware models and managers mentioned above for RCS Av's, and with the addition of the EGA model and a preliminary version of the EGA Manager. The bipropellant fill was **50%** which provides worst-case disturbances, and the pendulums were initialized to 20° from the Z-axis, which was derived from the requirement that the PMD control the propellant center of mass to 5 cm by the end of a short "quiescent" period immediatel y prior to main engine ignition. T 'hc pre-aim error was 10 per axis. Also simulated was a 2S0 mscc delay between main engine ignition and TVC enable which is necessary for power management. The first plot of Fig. 11 shows the history of the X-axis orientation angle, which was initialized at 6.2° to align the pre-aim'ed main engine with the Av target at the inertial coordinates [0 O - 1]. The large disturbance from the sloshing bipropellant is superposed on the slow guidance loop response, which slews the spacecraft attitude 10 to compensate for the pre-aim error. The plot below it shows the spacecraft rate, which peaks out at 0.30/s. The vibration of the magnetometer boom in response to the translational acceleration from the main engine gives this plot its "ratty" look. The third plot shows the engine deflection angle, rcfcrcnccd to the pre-aim orientation. The stead y-state shift of 10 points the engine thrust vector through the equilibrium systcm mass center, and the maximum deflection is almost 2.5° from the initial orientation, which can bc considered as a 1.5° overshoot. The final plot shows the combined fixed and proportional Av pointing errors as a function of burn duration. The curve labeled "requirement" corresponds to the allocation shown in 'J'able 4 below. Fig. 12. shows similar plots for the Y-axis.

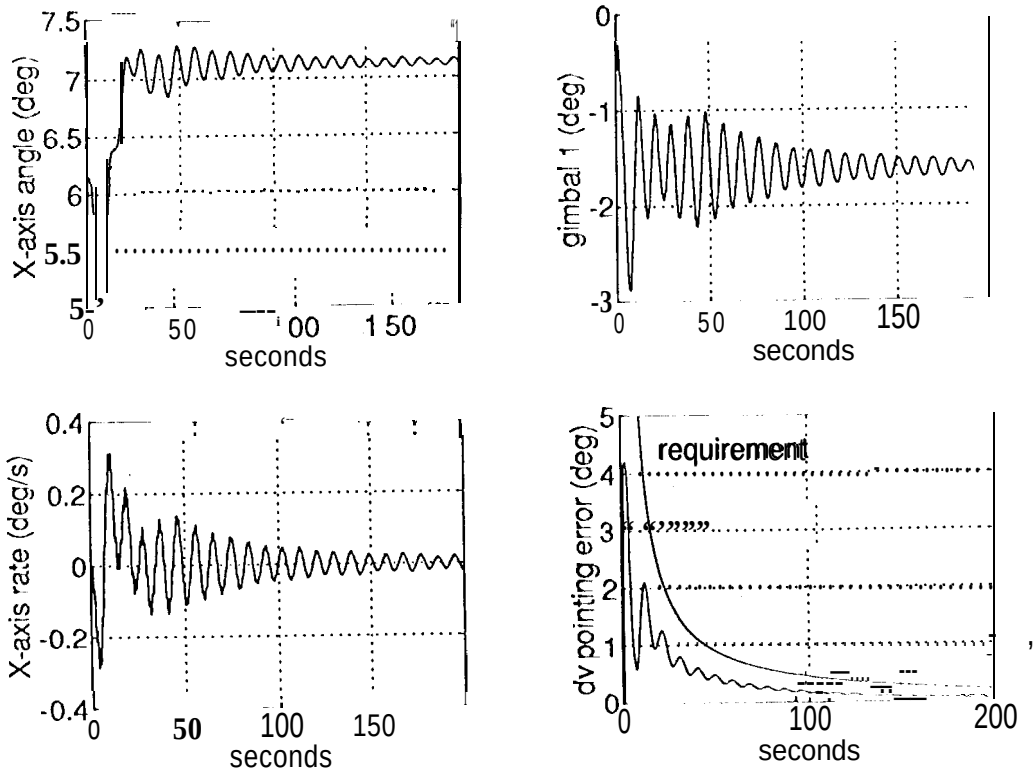

Fig. 11 Main Engine Δv Simulation (X-axis)

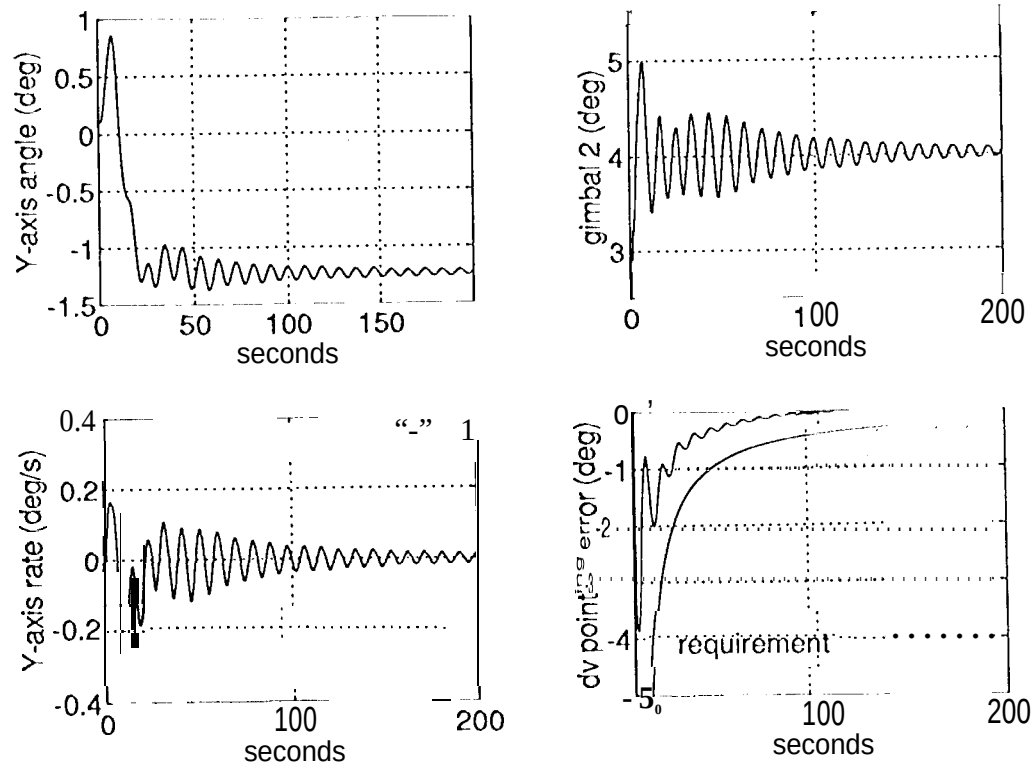

Fig. 12 Main Engine Δv Simulation (Y-axis)

Tables 3 and 4 summarize the maneuver error budgets. The fixed magnitude error is due to several sources, including uncertainties in turn-residual Av, main engine tail-off impulse, and the corruption of the accelerometer data by rotational accelerations. The proportional magnitude error is duc to accelerometer errors. The fixed pointing error is dominated by the TVC transient, as shown above in Fig. 10, and the proportional pointing error is mostly duc to misalignments of the main engine assembly. For long burns, gyro drift becomes an important contributor to Av pointing error (StarID data may not be available), and this case is handled separately.

error source	fixed error (mm/s)	proportional error (%)
probabilistic turn-residual AV [type-2 @0.75 deg/s]	9.0	----
rotational dynamics / engine articulation	13.2	0.0
post TVC recovery	11,0	----
propellant slosh	5.8	----
sensing axis misalignment	----	0.22
accelerometer errors:		
scale factor	----	0.15
bias	----	0.26
quantization	2.5	----
AV scheduling errors:		
valve command resolution	0.0	----
tailoff impulse prediction	10.0	----
TOTAL (RSS)	22.7	0.37
REQUIREMENT	30.0	1.05

Table 3 Main Engine Δv Magnitude Errors (3σ)

error source	fixed error (mm/s)	proportional error (mrad)
probabilistic turn-residual AV [type-2 @0.75 deg/s]	9.0	----
initial attitude determination:	----	4.0 (5.7)*
gyro scale factor / misalignments (1 80° turn)	----	1.6 (17.9)'
thrust vector articulation estimation:		
EGA / gimbals	----	5.3
engine thrust	----	10.0
PMS to S/C	----	5.0
thrust vector control behavior:		
TVC transients	37.5 (68.0)"	----
TVC steady-state	- - - -	1.0
SUB-TOTAL (RSS)	38.6 (68.6)**	13.2 (24.1)'
REQUIREMENT	52.5 (105.O)**	21.0
gyro drift (long burn)		17.1
TOTAL (RSS)		21.6 (29.6)*
REQUIREMENT (long burn)		30.0

** prior to pre-aim calibration

* prior to SRU/IRU calibration

Table 4 Main Engine AV Pointing Errors (3σ)

ACKNOWLEDGEMENTS

This research was carried out by the Jet Propulsion Laboratory, California Institute of Technology, under contract with the National Aeronautics and Space Administration.

REFERENCES

1. Cassini Project Mission Plan, PD 699- 100-2 Rev B, 12 March 93 (internal J}'], document D-5564, RCV B)

2. 1 Jackncy, J. C., D. Il. Bernard, and R.D. Rasmussen, "The Cassini Spacecraft: Object Oriented Flight Control Software," Paper No. A AS 93-033, 16th Annual A AS Guidance and Control Conference, 6-10 Feb 93, Keystone, Colo.

3. Brakke, K. A., "Surface Evolver Manual," Version 1.90,2 April 93, The Geometry Center, Minneapolis, Minn.

4. NASA SP-106, "The Dynamic Behavior of Liquids in Moving Containers," cd. by H.N. Abramson, 1966

5. SD-FAST User's Manual, Symbolic Dynamics, inc., Version B.1. 1, July 1991

6. Jain, A., "DARTS - Dynamics Algorithms for Real-l"imc Simulation of the CRAF/Cassini Spacecraft," January 1992 (internal JPL document D-9308)

7. Kirchwcy, C. B., and 1..1.. Sackett, "Stability of the Shuttle On-Orbit Flight Control System For a Class of Flexible Payloads," Paper No. 83-2178, AlAA Guidance and Control Conference, Gatlinburg, Tenn., Aug 1983.

8. Atherton, D. P., *Nonlinear Control Engineering*, Van Nostrand Reinhold, 1975

9. Enright, P. J,. "Thrust Vector Control Algorithm Design for the Cassini Spacecraft," Paper AIAA 93- 1043, Al AA/Al IS/ASEE Aerospace Design Conference, Irvine, Calif., Feb. 1993

10. Kopf, E.H., "A Mariner Orbiter Autopilot Design," NASA TR 32-1349, Jet Propulsion Laboratory, California Institute of Technology, 15 January 1969

11. Lurie, B., *Feedback Maximization*, Artech House, Dedham, Mass., 1986

12. Horowitz, I. M., Synthesis *of Feedback Systems*, Academic, New York, 1963